nature climate change

LETTERS

PUBLISHED ONLINE: 6 MARCH 2017 | DOI: 10.1038/NCLIMATE3239

The peak structure and future changes of the relationships between extreme precipitation and temperature

Guiling Wang[1]*, Dagang Wang[1,2]*, Kevin E. Trenberth[3], Amir Erfanian[1], Miao Yu[1,4], Michael G. Bosilovich[5] and Dana T. Parr[1]

Theoretical models predict that, in the absence of moisture limitation, extreme precipitation intensity could exponentially increase with temperatures at a rate determined by the Clausius–Clapeyron (C–C) relationship[1,2]. Climate models project a continuous increase of precipitation extremes for the twenty-first century over most of the globe[3–5]. However, some station observations suggest a negative scaling of extreme precipitation with very high temperatures[6–9], raising doubts about future increase of precipitation extremes. Here we show for the present-day climate over most of the globe, the curve relating daily precipitation extremes with local temperatures has a peak structure, increasing as expected at the low–medium range of temperature variations but decreasing at high temperatures. However, this peak-shaped relationship does not imply a potential upper limit for future precipitation extremes. Climate models project both the peak of extreme precipitation and the temperature at which it peaks (T_{peak}) will increase with warming; the two increases generally conform to the C–C scaling rate in mid- and high-latitudes, and to a super C–C scaling in most of the tropics. Because projected increases of local mean temperature (T_{mean}) far exceed projected increases of T_{peak} over land, the conventional approach of relating extreme precipitation to T_{mean} produces a misleading sub-C–C scaling rate.

Among the warming-induced hydrological changes, one of the most definitive and detectable changes is the increase of precipitation intensity[10]. Increases in precipitation intensity and in the frequency of heavy precipitation events have become widespread according to observational data[11,12]. More rain has fallen in extreme events[13], leading to more days with heavy precipitation and a disproportional amount of annual precipitation contributed by extremes[14]. Global and regional climate models driven with future scenarios of increasing CO_2 concentrations produce an increase of precipitation intensity and extremes as warming continues in the future[3–5]. An increase of extreme precipitation often takes place at the expense of light and moderate precipitation[15], leading to longer periods of continuous dry days and a generally higher fraction of precipitation that runs off, which increases both drought and flood risks[16,17]. It is therefore critical that we develop predictive understanding of future changes of precipitation extremes to inform and guide the development of long-term adaptation and mitigation strategies.

The C–C scaling, which describes the increase of atmospheric moisture holding capacity with temperature (at approximately 7% per degree Celsius of warming near the surface), has been widely considered as a guide for quantifying future increase of precipitation extremes[1,2]. Precipitation intensity is proportional to the surface atmospheric moisture content because it occurs mainly through convergence of the low-level moisture by the responsible storm or weather system. As precipitation extremes tend to take place when the atmosphere is close to saturation, the intensity of extreme precipitation is often proportional to the surface air moisture holding capacity too, which exponentially increases with temperature at the C–C scaling rate. As other processes and factors come into play[6,18], significant deviations from the C–C scaling have been found in the relationship between precipitation extremes and local temperature based on observational data[19–22]. More importantly, at many meteorological stations, precipitation extremes were found to decrease at the higher end of local temperature variations[6–9]. This apparent negative scaling with local temperature and its implications are poorly understood, and were considered 'controversial' in the Intergovernmental Panel for Climate Change (IPCC) 5th Assessment Report (AR5)[23]. If not properly characterized, the observed decrease of precipitation at the high temperature range could be misinterpreted as a suggestion for the potential existence of an upper limit for future precipitation extremes. Here we present a comprehensive global analysis to characterize the relationship between precipitation extremes and local temperatures, and how the relationship might change in the future. This is done based on multiple sources of gridded observational and reanalysis ('observational' hereafter) data, and output from the Representative Concentration Pathway 8.5 (RCP8.5) extended run (to 2300) of six global models participating in the Coupled Model Inter-comparison Project phase 5 (CMIP5) (see Methods).

In the context of climate variability, the decrease of daily precipitation extremes when local temperature exceeds a certain threshold is a robust characteristic across climate regimes, across different data sets, and across different climate models. As examples, Fig. 1 plots the daily precipitation extremes against the corresponding daily local temperature for eight sample areas that span different

[1]Department of Civil and Environmental Engineering & Center for Environmental Sciences and Engineering, University of Connecticut, Storrs, Connecticut 06269, USA. [2]School of Geography and Planning, Sun Yat-sen University, Guangzhou 510275, China. [3]National Center for Atmospheric Research, Boulder, Colorado 80307, USA. [4]Collaborative Innovation Center on Forecast and Evaluation of Meteorological Disasters, Nanjing University of Information Science and Technology, Nanjing 210044, China. [5]Global Modeling and Assimilation Office, NASA GSFC, Greenbelt, Maryland 20771, USA. *e-mail: guiling.wang@uconn.edu; wangdag@mail.sysu.edu.cn

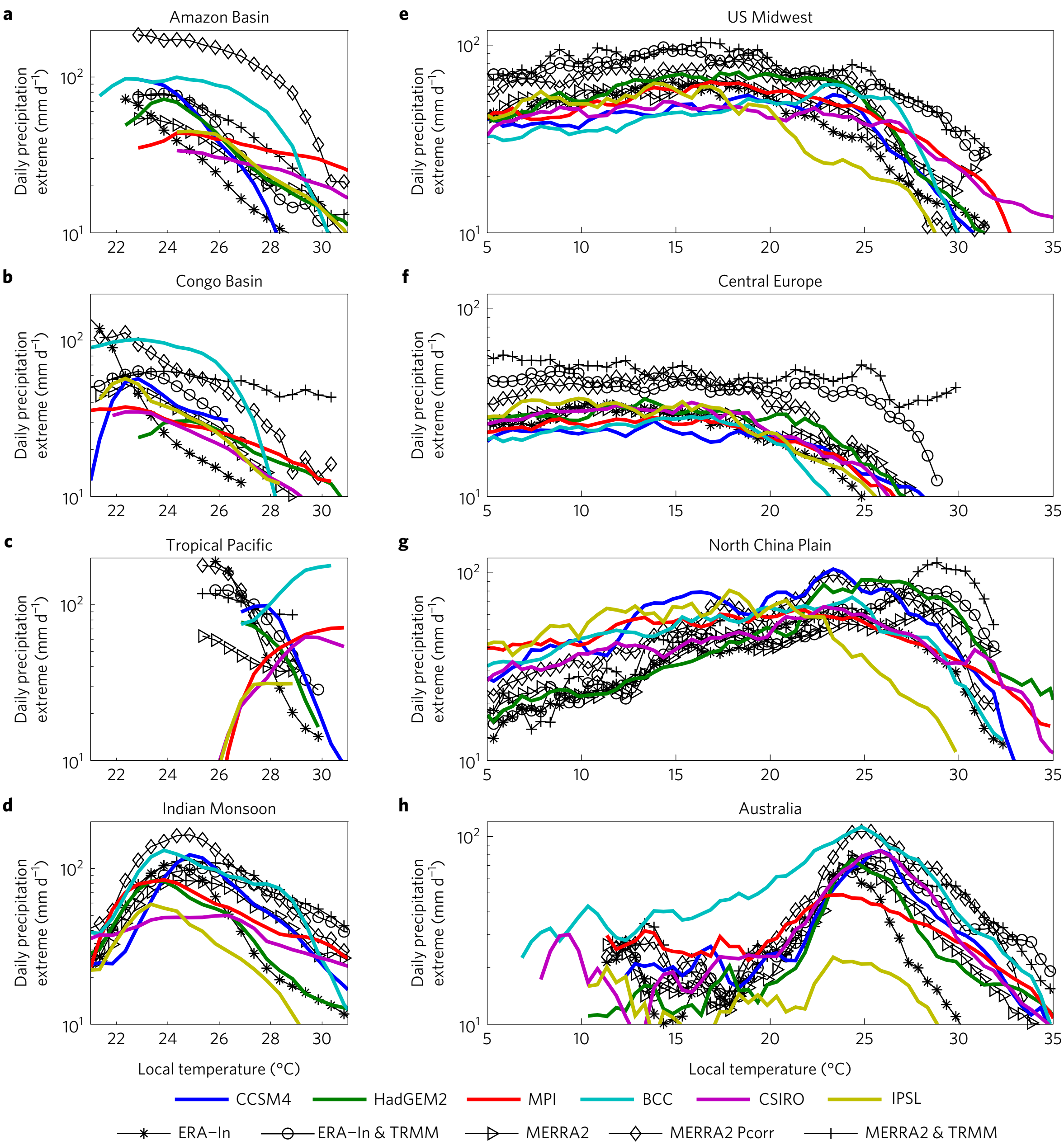

Figure 1 | Daily precipitation extremes varying with local temperature, estimated based on different sources of data, including observation-based and reanalysis data (black with symbols) as well as six global models (thick coloured lines) for eight sample areas. a, Amazon Basin (60° W, 0°). **b**, Congo Basin (22° E, 4° S). **c**, Tropical Pacific (150° E, 0°). **d**, Indian monsoon region (80° E, 20° N). **e**, US Midwest (90° W, 37° N). **f**, Central Europe (22° E, 47° N). **g**, North China Plain (117° E, 36° N). **h**, Australia (131° E, 20° S). Each sample area is made up of the nine grid points of the four grid cells surrounding the identified point (in parentheses). Note that the vertical axes have a logarithmic scale.

continents and climate regimes, including mid-latitude, tropical, monsoon, and non-monsoon climate. Over all sample areas, all observational data agree on a decrease of precipitation extremes with temperature at the high range of local temperature variation, and this decrease can occur without a decrease of specific humidity (Supplementary Fig. 1). The threshold temperature at which precipitation extreme peaks (T_{peak}) varies from region to region; an increasing branch of the curve at lower temperature may or may not be present, and would be absent if local temperature is always warmer than the threshold (for example, in Fig. 1a–c). When local temperature exceeds the threshold, precipitation extremes follow an approximately exponential decrease. Over most of the eight sample areas, all six models reproduce the general features of the extreme precipitation–temperature relationship, and the observational ensemble and the six-model ensemble overlap. One exception is the area in tropical Pacific, where all observational data produce a sharp decrease of precipitation extremes with temperature (that is, without an increasing branch), a feature well captured by CCSM4 and HadGEM2-ES whereas the other four models simulate an increase before it plateaus/decreases.

For all observational data examined, the decrease of precipitation extremes at relatively high local temperature is detected at all grid points over land and most grid points over oceans (Fig. 2a and Supplementary Fig. 2), with exceptions over scattered areas of tropical and extratropical oceans. The rate of decrease ranges from less than 10% per °C in mid- and high-latitudes over land to more than 50% per °C over some oceanic areas, and shows a distinct spatial pattern: faster over the tropics than extratropics

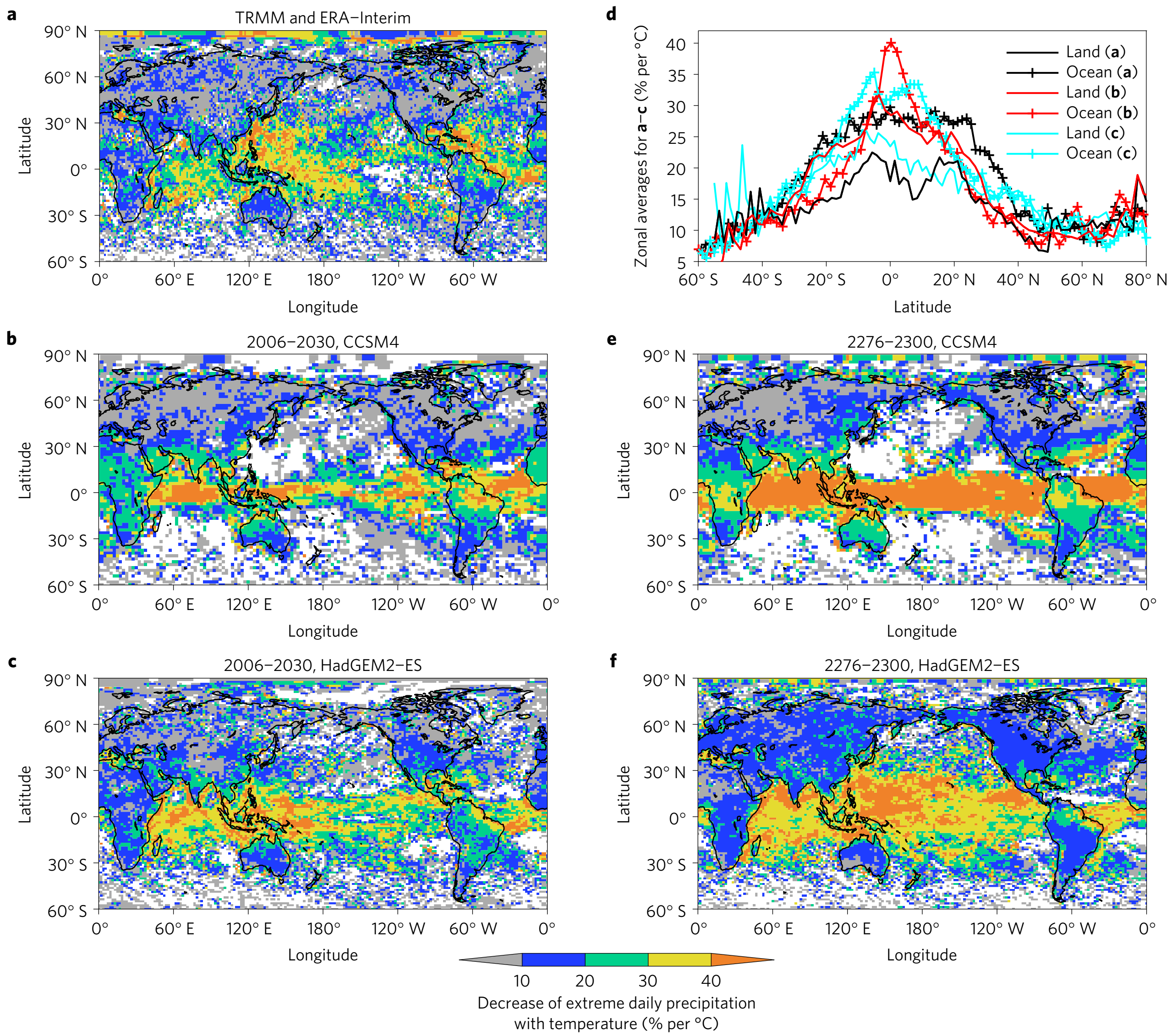

Figure 2 | Rate of decrease of extreme daily precipitation with local temperature at the high temperature range. a, Based on precipitation from TRMM 3B42 and near-surface air temperature from the ERA-Interim data over 50° S–50° N, and based on ERA-Interim precipitation and temperature data over higher latitudes. **b**,**c**,**e**,**f**, Based on output from the RCP8.5 runs of CCSM4 and HadGEM2-ES for the periods 2006–2030 and 2276–2300, respectively. **d**, Zonal average over land and ocean for **a**–**c**. Over the unshaded areas, a decrease of extreme precipitation at high temperature was not detected.

and faster over tropical oceans than tropical land (Fig. 2d). Both the land–ocean contrast and the tropics–extratropics contrast are captured by most of the models (Fig. 2 and Supplementary Fig. 3). The magnitude and spatial pattern of the decreasing rate of daily extremes estimated for the present climate of the six models span a similar range of variations to those of the observational data. The only difference that stands out is that climate models collectively overestimate the portion of tropical oceans where a decrease of precipitation extremes at high temperature is not detected for the present climate. The peak value of precipitation extremes (P_{peak}) varies substantially among the different data sets and different models; however, for all data and all models, the threshold temperature (T_{peak}) at which the daily precipitation extreme peaks is highly zonally symmetric, approximately in the range of 25–30 °C over tropical oceans, 20–25 °C over tropical land, and 10–20 °C over most mid- and high-latitudes (Supplementary Figs 4 and 5).

Clearly, the concurrence of relatively high (low) precipitation extremes and relatively low (high) local temperature is a globally relevant phenomenon that is robust across different data sets and well captured by climate models. It can result from several mechanisms working together, of which the primary two are moisture limitation for precipitation at high temperature, and temperature response to precipitation (rather than the other way around). In the first case, very high temperature may mean a large saturation deficit, which may inhibit the development of deep convection and therefore extreme precipitation. In this situation, low or lack of precipitation is a result of high temperature with insufficient moisture. This can arise over land, for instance, if the primary moisture source is the ocean (where temperature is typically lower than land during warm seasons, leading to a drop of relative humidity over land). In the second case, in anticyclonic or 'settled' conditions, convective clouds and precipitation are suppressed, leading to more sunshine, lighter winds and smaller surface evaporative fluxes, and thus higher surface temperatures; on the other hand, in cases of extreme precipitation events, the cloud radiative effect, strong latent heat fluxes and, in the case of the ocean, strong mixing, all contribute to surface cooling. In these situations, temperature variations result from the presence or absence of precipitation. Both mechanisms are important in shaping the documented relationship between precipitation extremes and temperature, as analysis based on temporally shifted

NATURE CLIMATE CHANGE DOI: 10.1038/NCLIMATE3239

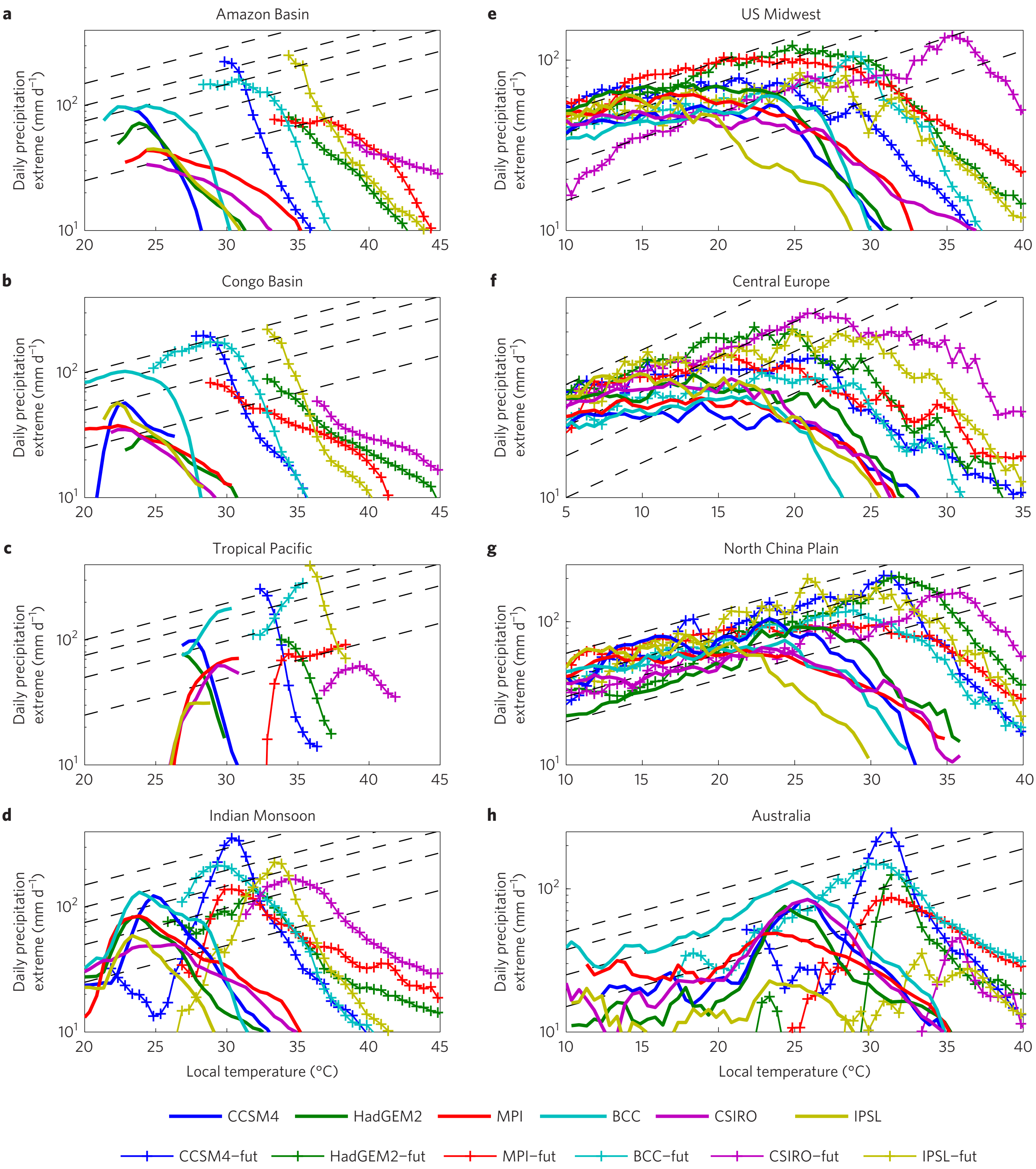

Figure 3 | Similar to Fig. 1, but based on output from six global models' RCP8.5 future run for the period 2276–2300 (thin coloured lines with plus symbols), in comparison with the period 2006–2030 (thick coloured lines). The black dashed lines plot the C–C scaling curves as a reference. Note that the vertical axes have a logarithmic scale and differ between panels.

data in both directions (with temperature leading or lagging precipitation by one day) produced qualitatively similar results. These processes/mechanisms discussed here are simulated in the CMIP5 RCP8.5 runs; in the reanalysis systems, the effects of precipitation causing temperature variations are not completely captured over the ocean due to the use of prescribed sea surface temperature.

The negative scaling at high temperatures does not refute the relevance of the C–C scaling. As a metric for precipitation intensity–temperature relationship, C–C scaling is applicable only when there is no moisture limitation (for example, when air is close to saturation) or when relative humidity is constant, which is not the case at the high range of temperature variation. Instead, based on both observational data and global models used in this study, the highest level of relative humidity tends to coincide with the peak of extreme precipitation intensity (and therefore takes place at the lower or medium range of temperature variation). As temperatures further increase, the increase of specific humidity with temperature slows down or plateaus, and hence relative humidity decreases (Supplementary Fig. 1). The condition at the peak of extreme precipitation is the closest for the C–C scaling to be applicable, and should be the object of analysis when characterizing the water cycle in a warming climate with reference to the C–C scaling rate.

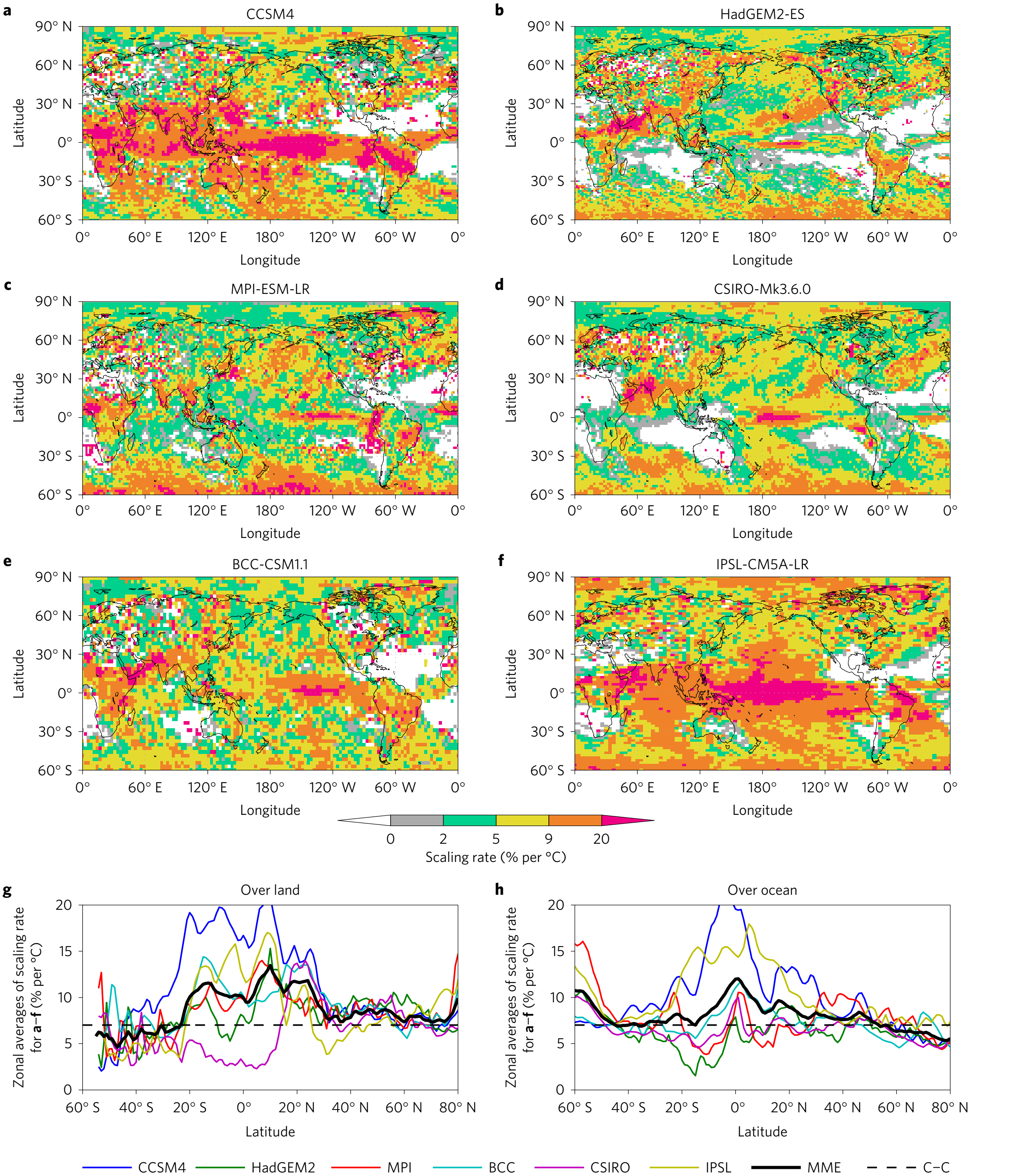

Figure 4 | The scaling rate of the peak of daily precipitation extreme (P_{peak}) with temperature at which it peaks (T_{peak}). a–f, Based on changes between 2006–2030 and 2276–2300 from each of the six models' RCP8.5 runs. **g**,**h**, Zonal averages of the scaling rate (% per °C) for each model and for the multi-model ensemble average (MME), plotted against the C–C scaling rate as a reference, over land and ocean, respectively. Over the unshaded areas in **a–f**, the peak of extreme precipitation is projected to decrease.

Comparison between present and future climates of the six models reveals several noticeable changes. In the future climate, the negative scaling rate of precipitation extremes with temperature would increase in magnitude over most of the tropical oceans, and the oceanic areas where negative scaling can be detected would expand, especially in CCSM4, HadGEM-ESM, CSIRO-MK3.6.0 and IPSL-CM5A-LR models (Fig. 2 and Supplementary Fig. 3). Qualitatively, the tropics–extratropics contrast and land–ocean contrast of the negative scaling rate in the future would remain similar to the present climate. However, over most of the globe, both the peak of precipitation extremes (P_{peak}) and the temperature at which it peaks (T_{peak}) would significantly increase (Supplementary Fig. 6); exceptions are found primarily in the subtropics, where extreme precipitation is projected to decrease due to circulation changes[24].

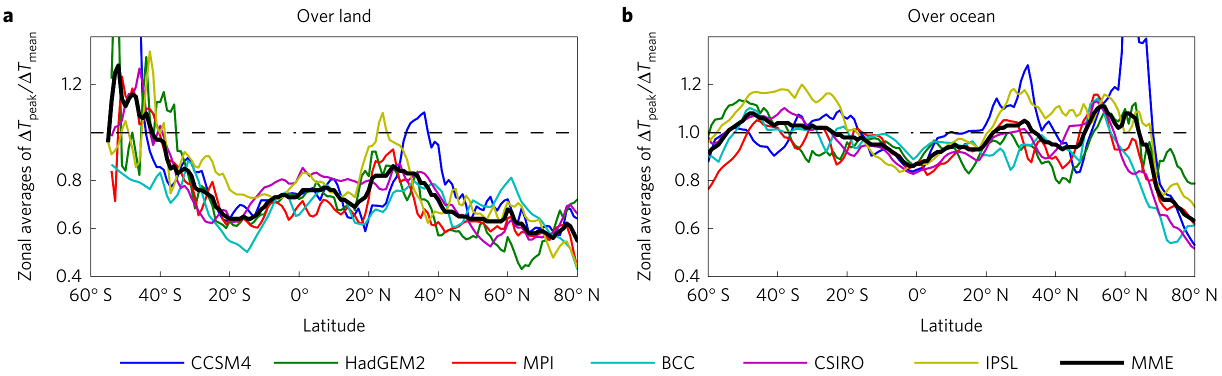

Figure 5 | Zonal averages of the ratio between T_{peak} changes and T_{mean} changes, based on differences between 2006–2030 and 2276–2300. a,b, Over land and over ocean, respectively, for each of the six models and for the multi-model ensemble mean (MME). Here T_{peak} is the temperature at which extreme precipitation peaks and T_{mean} is the local mean temperature.

Details of the relationship in the future climate and how it compares with the present climate are shown in Fig. 3 using the same eight sample areas as in Fig. 1. In all models and for all eight sample areas, the peak of precipitation extremes would increase in magnitude and occur under higher temperature in the future. For most areas in most models, regardless of the slope of the curve's increasing branch (if one exists), the present and future peaks tend to fall on the same C–C line and therefore scale approximately at the C–C rate. If the increasing branch is roughly along the C–C scaling line (for example, in the US Midwest and North China Plains), it would extend to the right in the future; and if the increasing branch has a steeper slope than the C–C scaling line (for example, in the Indian monsoon and Australian areas), it would shift to the right in the future, which adds to the emerging evidence that future changes cannot simply be extrapolated from present-day scaling[25,26]. For most areas and most models, the decreasing branch in future and present climates are roughly parallel. Exceptions are found for the tropical Pacific area, where some models simulate a primarily increasing branch for the present climate and a primarily decreasing branch for the future climate.

Despite the remarkable cross-model similarity in the spatial patterns of P_{peak} and T_{peak} in present climate, the projected future changes bear little similarity among the models (Supplementary Fig. 6), reflecting the high degree of model-related uncertainty in projecting future climate changes[27]. However, combining the projected changes of the two variables, the rate of P_{peak} increasing with T_{peak} varies within a rather narrow range and shows inter-model similarity in the spatial pattern (Fig. 4). The scaling of P_{peak} with T_{peak} based on the multi-model ensemble average is in the range of 5–10% per °C (close to the C–C rate) in most of the mid- and high-latitudes over both land and ocean, but reflects a super C–C rate of more than 10% per °C (with stronger model dependence) in most of the tropics and over the ocean near Antarctica (Fig. 4). This tropics–extratropics contrast is similar to findings from previous studies[18,28].

The scaling rate found in this study is substantially higher than those found in conventional studies linking unconditional precipitation extremes ($P_{extreme}$, defined with no regard to temperature, see Methods) with local mean temperature (T_{mean}) (for example, refs 18,28,29 and the references therein). In the present climate, T_{peak} is higher than T_{mean} over the mid- and high-latitudes, and lower than T_{mean} over most tropical and subtropical land; for future changes, the projected increase of T_{peak} is significantly slower than that of T_{mean} across the global land and over part of tropical oceans in all six models (Fig. 5 and Supplementary Figs 7 and 8). On the other hand, the projected relative increases of $P_{extreme}$ are similar to or smaller than those of P_{peak}. Therefore, linking $P_{extreme}$ with T_{mean} yields a spuriously low scaling rate (2–5% per °C over land, Supplementary Figs 8 and 9) that is not directly related to any specific process or to C–C scaling. Both the slower warming of T_{peak} than T_{mean} over land and the low $P_{extreme}$-versus-T_{mean} scaling rate are reflections of a general decrease of relative humidity over land as the Earth warms, a result of ocean being the primary moisture source and enhanced mean warming over land compared to oceans[29,30].

In conclusion, the C–C scaling rate is found to be a highly relevant constraint on precipitation extremes in a warming climate. Multiple mechanisms contribute to shape the peak-shaped precipitation–temperature relationship, and which one is dominant is likely to be region-specific. Although the decrease of precipitation extremes at high range of local temperature variation does not seem to have direct implication for future precipitation changes, understanding its causes will help tackle why models differ so much in their capability to reproduce this phenomenon over tropical oceans and may lead to new ways to improve climate model performance.

Methods

Methods, including statements of data availability and any associated accession codes and references, are available in the online version of this paper.

Received 3 October 2016; accepted 2 February 2017; published online 6 March 2017

References

1. Trenberth, K. Conceptual framework for changes of extremes of the hydrologic cycle with climate change. *Climatic Change* **42,** 327–339 (1999).
2. Trenberth, K., Dai, A., Rasmsussen, R. & Parsons, D. The changing character of precipitation. *Bull. Am. Meteorol. Soc.* **84,** 1205–1217 (2003).
3. Tebaldi, C., Hayhoe, K., Arblaster, J. & Meehl, G. Going to the extremes. *Climatic Change* **79,** 185–211 (2006).
4. Kharin, V. V. *et al*. Changes in temperature and precipitation extremes in the IPCC ensemble of global coupled model simulations. *J. Clim.* **20,** 1419–1444 (2007).
5. Kharin, V. V., Zwiers, F. W., Zhang, X. & Wehner, M. Changes in the temperature and precipitation extremes in the CMIP5 ensemble. *Climatic Change* **119,** 345–357 (2013).
6. Berg, P. *et al*. Seasonal characteristics of the relationship between daily precipitation intensity and surface temperature. *J. Geophys. Res.* **114,** D18102 (2009).
7. Hardwick Jones, R. *et al*. Observed relationships between extreme sub-daily precipitation, surface temperature, and relative humidity. *Geophys. Res. Lett.* **37,** L22805 (2010).
8. Utsumi, N. *et al*. Does higher surface temperature intensify extreme precipitation? *Geophys. Res. Lett.* **38,** L16708 (2011).
9. Maeda, E. E. *et al*. Decreasing precipitation extremes at higher temperatures in tropical regions. *Nat. Hazards* **64,** 935–941 (2012).
10. Hegerl, G. E. *et al*. Challenges in quantifying changes in the global water cycle. *Bull. Am. Meteorol. Soc.* **96,** 1097–1115 (2015).

11. Groisman, P. *et al*. Trends in intense precipitation in the climate record. *J. Clim.* **18,** 1326–1350 (2005).
12. Fischer, E. M. & Kutti, R. Observed heavy precipitation increase confirms theory and early models. *Nat. Clim. Change* **6,** 986–991 (2016).
13. Huntington, T. G., Richardson, A. D., McGuire, K. J. & Hayhoe, K. Review: climate and hydrological changes in the northeastern United States: recent trends and implications for forested and aquatic ecosystems. *Can. J. Forest Res.* **39,** 199–212 (2009).
14. Easterling, D. R. *et al*. Climate extremes: observations, modeling and impacts. *Science* **289,** 2068–2074 (2000).
15. Allan, R. & Soden, B. Atmospheric warming and amplification of precipitation extremes. *Science* **321,** 1481–1484 (2008).
16. Ahmed, K. F. *et al*. Statistical downscaling and bias correction of climate model outputs for climate change impact assessment in the U.S. Northeast. *Glob. Planet. Change* **100,** 320–332 (2013).
17. Parr, D. T., Wang, G. L. & Bjerklie, D. Integrating remote sensing data on evapotranspiration and leaf area index with hydrological modeling: impacts on model performance and future predictions. *J. Hydrometeorol.* **16,** 2086–2100 (2015).
18. O'Gorman, P. A. Precipitation extremes under climate change. *Curr. Clim. Change Rep.* **1,** 49–59 (2015).
19. Lenderink, G. *et al*. Scaling and trends of hourly precipitation extremes in two different climate zones—Hong Kong and the Netherlands. *Hydro. Earth Syst. Sci.* **15,** 3033–3041 (2011).
20. Lenderink, G. & van Meijgaard, E. Increase in hourly precipitation extremes beyond expectations from temperature changes. *Nat. Geosci.* **1,** 511–514 (2008).
21. Shaw, S. B. *et al*. The relationship between extreme hourly precipitation and surface temperature in different hydroclimatic regions of the United States. *J. Hydrometeorol.* **12,** 319–325 (2011).
22. Mishra, V. *et al*. Relationship between hourly extreme precipitation and local air temperature in the United States. *Geophys. Res. Lett.* **39,** L16403 (2012).
23. Boucher, O. *et al*. in *Climate Change 2013: The Physical Science Basis* (eds Stocker, T. F. *et al*.) 571–657 (IPCC, Cambridge Univ. Press, 2013).
24. Seager, R., Naik, N. & Vecchi, G. A. Thermodynamic and dynamic mechanisms for large-scale changes in the hydrological cycle in response to global warming. *J. Clim.* **23,** 4651–4668 (2010).
25. Ban, N., Schmidli, J. & Schär, C. Heavy precipitation in a changing climate: does short-term summer precipitation increase faster? *Geophys. Res. Lett.* **42,** 1165–1172 (2015).
26. Chan, S. C. *et al*. Downturn in scaling of UK extreme rainfall with temperature for future hottest days. *Nat. Geosci.* **9,** 24–28 (2016).
27. Christensen, J. H. *et al*. in *Climate Change 2013: The Physical Science Basis* (ed. Stocker, T. F.) 1217–1308 (IPCC, Cambridge Univ. Press, 2013).
28. O'Gorman, P. A. Sensitivity of tropical precipitation extremes to climate change. *Nat. Geosci.* **5,** 697–700 (2012).
29. O'Gorman, P. A. & Schneider, T. The physical basis for increases in precipitation extremes in simulations of 21st-century climate change. *Proc. Natl Acad. Sci. USA* **106,** 14773–14777 (2009).
30. Sherwood, S. & Fu, Q. A drier future? *Science* **343,** 737–739 (2014).

Acknowledgements

This study was supported by funding from the US National Science Foundation to G.W. (AGS-1063986, AGS-1659953). D.W. was supported by funding from the National Natural Science Foundation of China (Grant No. 51379224). K.E.T. is partially sponsored by DOE grant DE-SC0012711 and NCAR is sponsored by the National Science Foundation. We acknowledge the World Climate Research Programme's Working Group on Coupled Modelling, which is responsible for CMIP. We also thank the climate modelling groups for producing and making their model output available. For CMIP the US Department of Energy's Program for Climate Diagnosis and Intercomparison provides coordinating support and led development of software infrastructure in partnership with the Global Organization for Earth System Science Portals.

Author contributions

G.W. and D.W. motivated the study; G.W. designed the study and conducted data analysis with input from K.E.T., M.G.B. and D.W.; G.W. and K.E.T. wrote the paper; A.E., D.T.P., D.W. and M.Y. all contributed to data processing.

Additional information

Supplementary information is available in the online version of the paper. Reprints and permissions information is available online at www.nature.com/reprints. Correspondence and requests for materials should be addressed to G.W. or D.W.

Competing financial interests

The authors declare no competing financial interests.

Methods

Three gridded observational/reanalysis data sets are used: the European Centre for Medium-Range Weather Forecasts (ECMWF) Re-analysis-Interim data (ERA-Interim)[31], at approximately 0.7° (lat) × 0.7° (lon) resolution globally; the NASA Modern Era Reanalysis for Research and Applications version 2 data (MERRA-2)[32], at 0.5° (lat) × 0.625° (lon) resolution globally; and the Tropical Rainfall Measuring Mission (TRMM) 3B42 precipitation data (version 7), which is a TRMM- and raingauge-adjusted multi-satellite precipitation rate product, available at 0.25° (lat) × 0.25° (lon) resolution covering the latitude band 50° S–50° N. Note that precipitation from ERA-Interim is model-simulated; MERRA-2 provides two estimates of precipitation, one simulated by the model in the reanalysis system (P_{model}) and one with the model biases corrected based on both gauge and satellite remote sensing data (P_{corr})[33]. These data sets support five combinations of past data, including two that pair ERA-Interim 2-m surface air temperature with ERA-Interim precipitation and with TRMM 3B42 precipitation, respectively, and three that pair the MERRA-2 lowest model level atmospheric temperature with MERRA-2 P_{model}, MERRA-2 P_{corr}, and TRMM 3B42 precipitation, respectively. The lowest model level temperature from MERRA-2 is chosen over 2-m temperature because MERRA-2 does not assimilate 2-m air temperature whereas ERA-Interim does. From the two reanalysis products, 25 years of data for the period 1991–2015 were used. Because the TRMM 3B42 precipitation data are available only from 1998 on, analyses involving TRMM 3B42 data were conducted over the period 1998–2015. In the global analysis of this study, to overcome the computer memory constraint and to achieve a spatial resolution similar to the climate models used, the reanalysis data were resampled to a coarser resolution by skipping every other grid point in each direction, leading to a resolution of roughly 1.40° (lat) × 1.40° (lon) used for the ERA-Interim data and 1.0° (lat) × 1.25° (lon) used for the MERRA-2 data; and the TRMM 3B42 precipitation data were resampled to match the grid system used for each reanalysis product. This resampling has negligible impact on the results of the analysis. To preserve the characteristics of precipitation extremes, no spatial interpolation is conducted, and resampling takes the raw data from the closest grid point.

Output from six global models is used, including CCSM4, HadGEM2-ES, MPI-ESM-LR, CSIRO-MK3.6.0, BCC-CSM1.1, and IPSL-CM5A-LR. These are the complete set of the Coupled Model Inter-comparison Project phase 5 (CMIP5) models for which the Representative Concentration Pathway 8.5 (RCP8.5) run was extended to the year 2300 with daily temperature and precipitation data available. The extended RCP8.5 run is necessary to ensure a meaningful signal on how the extreme precipitation–temperature relationship might change in a warming climate. Model output during the period 2006–2030 is used for the model present climate, and the period 2276–2300 for the model future climate. With the exception of the CCSM4 model, for which the output was resampled by skipping every other grid point in each direction, for all others the native spatial resolution of each model was used. Instead of limiting the analysis of the model and observational data to the period of CMIP5 historical runs (that end in 2005), here the 2006–2030 RCP8.5 period is used to represent the model 'present' climate, for comparison with the 1991–2015 observational period (1998–2015 for TRMM). This is desirable because more (and presumably better quality) observational data from recent years have been assimilated to the reanalysis systems (of both ERA-Interim and MERRA-2). It is also desirable to extend the record to 25 years for statistical robustness. The incomplete overlap between observational and model periods does not pose a problem for their comparison because the extreme precipitation–temperature relationship curve does not show detectable changes over the course of one or two decades.

All analyses were conducted based on daily data. The definition of daily precipitation extremes for each grid cell is conditional on local temperature. First, all daily precipitation at four grid points of the same grid cell within the analysis period are 'binned' according to the corresponding temperature at each grid point, and a temperature bin size of 0.5 °C is used. Within each temperature bin that contains more than 100 data points, daily precipitation data are then analysed to estimate the 99th percentile, and those exceeding the 99th percentile are averaged to define the daily extreme for each bin temperature; for bins with less than 100 data points (which occurs only at the lowest and highest ends of temperature range), statistics for precipitation extreme are set to missing value. The resulting daily extremes corresponding to different bin temperatures are then smoothed using 3-bin moving-window averaging, and the resulting statistics are used to characterize the scaling relationship, to define the peak of extreme precipitation intensity (P_{peak}) and the local temperature at which it peaks (T_{peak}), and to estimate the exponential decreasing rate if a decrease of precipitation extremes at high temperature is detected. The exponential rate of decrease is calculated over the temperature range between T_{peak} and the temperature 1 °C below T_{max}, where T_{max} is the highest bin temperature for which there is sufficient data to support the definition of a precipitation extreme.

To estimate the exponential scaling rate (r) underlying a change of extreme precipitation from P_a to P_b when temperature increases from T_a to T_b, two different approaches can be used. One describes the relationship empirically as $P_b = P_a(1+r_1)^{(T_b-T_a)}$ (ref. 7), and hence the scaling rate r_1 can be estimated as:

$$r_1 = (e^{\frac{\ln P_b - \ln P_a}{T_b - T_a}} - 1) \times 100\% \quad (1)$$

The other makes use of the approximate form of the Clausius–Clapeyron equation and describes the relationship as $P_b = P_a e^{r_2(T_b-T_a)}$ (ref. 34) and hence the scaling rate r_2 can be estimated as:

$$r_2 = \frac{\ln P_b - \ln P_a}{T_b - T_a} \times 100\% \quad (2)$$

Equation (2) would be more appropriate when it is assumed a priori that thermodynamics (therefore C–C scaling) dominates the difference between P_a and P_b, which is not necessarily the case here. Therefore, in this study, equation (1) is used to estimate the scaling rate on the decreasing branch of the extreme precipitation–temperature curve for the present-day climate, which is negative and its absolute value is presented in Fig. 2 and Supplementary Figs 2 and 3. Equation (1) is also used to estimate the rate of P_{peak} scaling with T_{peak} based on their changes between present and future climates, which is mostly positive as shown in Fig. 4. Note that $r_2 = \ln(1+r_1)$, and for $|r_1| < 1$, the Maclaurin series $\ln(1+r_1) = r_1 - (r_1^2/2) + (r_1^3/3) - (r_1^4/4) + \ldots$. Within the typical range of the C–C scaling rate (5–10% per °C)[23], higher-order terms are small and first-order approximation leads to $r_1 \approx r_2$. Therefore the two approaches produce largely similar results.

The extreme precipitation analysis described above can be done with data that lump all days of the years together, or with data for days of specific season(s) only. Qualitatively the nature of the scaling relationship does not show clear seasonal dependency; quantitatively, results based on the lumped data (as used in this study) are dominated by data from the warm season (when convective precipitation is dominant).

For any given criterion of extreme definition (for example, daily precipitation exceeding the 99th percentile), instead of defining precipitation extremes conditional on temperature (as is done for this study), unconditional precipitation extremes were widely used in previous studies. The unconditional approach defines the 99th percentile of precipitation based on all data points with no regard to temperature, and the days with precipitation exceeding the 99th percentile are extracted as the extreme days, and average among these days defines the unconditional extreme ($P_{extreme}$). Past studies evaluating the scaling of precipitation extremes with local temperature were mostly based on $P_{extreme}$ and local mean surface temperature (T_{mean}) (see reviews in ref. 18).

In defining both conditional and unconditional extremes, the definition of 99th percentile in this study is based on all days and not just the rain days. For applications in assessing changes of precipitation extremes, definition based on all-day percentiles was recommended over the wet-day percentiles[35].

Data availability. All data analysed in this study are publicly available. The ERA-Interim data was obtained from the NCAR Research Data Archive (https://doi.org/10.5065/D64747WN); the MERRA-2 data is available from NASA Goddard Earth Sciences (GES) Data and Information Services Center (DISC) at https://disc.sci.gsfc.nasa.gov/mdisc; and the TRMM 3B42 data is available from GES DISC at https://disc.gsfc.nasa.gov/precipitation. The Global climate models output can be obtained from the CMIP5 archive accessed through the Earth System Grid Federation data portal (http://esgf.llnl.gov).

References

31. Dee, D. P. *et al*. The ERA-Interim reanalysis: configuration and performance of the data assimilation system. *Q. J. R. Meteorol. Soc.* **137,** 553–597 (2011).
32. Bosilovich, M. *et al*. *MERRA-2: Initial Evaluation of the Climate* NASA/TM–2015-104606 Vol. 43 (NASA GSFC, 2015).
33. Reichle, R. H. & Liu, Q. *Observation-Corrected Precipitation Estimates in GEOS-5* NASA/TM–2014-104606 Vol. 35 (NASA GSFC, 2014).
34. Lorenz, D. J. & DeWeaver, E. T. The response of the extratropical hydrological cycle to global warming. *J. Clim.* **20,** 3470–3484 (2007).
35. Schär, C. *et al*. Percentile indices for assessing changes in heavy precipitation events. *Climatic Change* **137,** 201–216 (2016).